UNIVERSITY OF BIRMINGHAM

Post processing of 3D printed metal scaffolds

Ginestra, Paola; Ceretti, Elisabetta; Lobo, David; Lowther, Morgan; Cruchley, Sam; Kuehne, Sarah; Villapun, Victor; Cox, Sophie; Grover, Liam; Shepherd, Duncan; Attallah, Moataz; Addison, Owen; Webber, Mark

[Link to publication on Research at Birmingham portal](#)

23rd International Conference on Material Forming (ESAFORM 2020)

Post Processing of 3D Printed Metal Scaffolds: a Preliminary Study of Antimicrobial Efficiency

Paola Ginestra[a]*, Elisabetta Ceretti[a], David Lobo[a], Morgan Lowther[b], Sam Cruchley[c], Sarah Kuehne[d], Victor Villapun[b], Sophie Cox[b], Liam Grover[b], Duncan Shepherd[e], Moataz Attallah[c], Owen Addison[d], Mark Webber [f]

[a]*Department of Mechanical and Industrial Engineering, University of Brescia, Via Branze 38, 25123 Brescia, Italy.*
[b]*School of Chemical Engineering, University of Birmingham, Edgbaston, Birmingham B15 2TT, UK.*
[c]*School of Metallurgy and Materials, University of Birmingham, Edgbaston, Birmingham B15 2TT, UK.*
[d] *School of Dentistry, University of Birmingham, 5 Mill Pool Way, Edgbaston, Birmingham B5 7EG, UK.*
[e]*Department of Mechanical Engineering, University of Birmingham, 5 Mill Pool Way, Edgbaston, Birmingham B5 7EG, UK.*
[f]*School of Biosciences, University of Birmingham, Edgbaston, Birmingham B15 2TT, UK.*

* Corresponding author. *E-mail address:* paola.ginestra@unibs.it

Abstract

Additive manufacturing techniques enable users to produce complex devices that would not be possible by conventional methods, offering unique advantages to the medical industry due to the possibility to customize devices to accurately fit patient geometries. The process as done today needs still to be optimized in many aspects to achieve implants which better meet the requirements of the end application. Both the surface and the mechanical properties of the implant device have to better mimic the properties of the anatomical region of interest to assure a good interconnection with the surrounding tissue and the development of a strong interface. In the case of complex implants, the geometric accuracy of the replacing device is not the only factor with regard to the specific patient need. An optimal surface treatment after the manufacturing process can lead to a highly improved interaction of the implant with the surrounding physiological tissue. The improved outcome will be beneficial for the patient recovery process after the operation. This work goal is to provide an optimization of the post processing process of 3D printed titanium implants and the improvement of their performances, by a better and shorter assimilation of the implant to achieve the optimal patient wellness. In particular, the paper aims at the preliminary identification of the proper surface treatments that can lead to an implant that promotes the reduction of the bacterial adhesion to allow a better osseointegration in a long-term period. Ti6Al4V samples have been produced by a Selective Laser Melting (SLM) machine and the as-built surfaces have been treated in order to analyze the effects of post-processing on the surface and antimicrobial properties of the 3D printed specimens.

Keywords: Type your keywords here, separated by semicolons ;

1. Introduction

The ability of Additive Manufacturing (AM) to produce small batches of highly customized and complex parts coupled with the reduction in the supply chain and lower lead times may be one of the answers to cope with the expected increase in implantable devices [1,2,3,4]. The limited size of printed parts does not normally pose a problem for AM implementation in healthcare, but the rough surface finish and isotropic microstructure of as build parts have required the use of post processing to obtain a satisfactory product [5]. The predominant materials in implantable devices are Stainless steel, Titanium alloys, Co-Cr-Mo, polymers [6,7,8,9] and some ceramics (alumina, zirconia and hydroxyapatite) [10], but the corrosion resistance, biocompatibility and lower stiffness in relation to other

metallic alloys resulting in lower stress shielding has led to a predominate use of Ti based alloys in AM focused in healthcare markets [11]. First implantable devices were considered adequate if they were durable, biocompatible and able to sustain the mechanical stresses imposed during service, however, history has shown that a high-quality implant must also hinder bacteria and soft tissue adhesion, while encouraging bone forming cell bonding and differentiation (i.e osteoblast) [12]. The ability of additive manufactured titanium to comply with all requirements is still dependent on the use of post processing to tune its structure and modify its surface finish (i.e. polishing). The impact of common industrial processes in bacteria and cell attachment is still mostly unknown and they have to be carefully selected as already demonstrated [13]. Infection of implantable devices is, still today, a great healthcare concern. Each year 1 to 5 % indwelling prosthetics became infected [14]. Antimicrobial coatings, photocatalysis antibodies and antibiotics can be applied to titanium surfaces to add an active mechanism of defense against bacteria colonization [15], but they are time consuming and complicate the part processing and supply chain. Polishing, etching, sandblasting and vibratory finishing are commercially available treatments implementable with relatively ease. Their low cost, practicality and simplicity make them ideal candidates to treat additive manufactured parts. In this paper, we propose the use of sandblasting and vibratory finishing treatments in as-build Ti6Al4V (Ti64) samples as a mean to reduce bacteria colonization. In particular, the Ti64 samples are produced by Selective Laser Melting (SLM) process and two strains of bacteria, S. epidermidis and P. aeruginosa are used to understand the possibility to guide the biofilm formation by tailoring the roughness and hydrophilicity of the surfaces.

2. Manufacturing

2.1. Powder characterization

The chemical composition of the Ti16Al4V powder was carried out by AMG Superalloys UK Ltd.

The morphology of the powder particles was determined by using a TM3000 Scanning Electron microscope (PHILIPS, US). Three powder samples were carefully mounted on a double carbon tape and the secondary electron mode was used to examine the surfaces and shapes of the particles.

To determine the particle size distribution (PSD), a HELLOS/BR (Sympatec GmbH, DE) laser diffraction system was used. This method allows the measurement of the distribution of large numbers of particles by analyzing the diffraction pattern of laser light to obtain statistically significant particle counts.

The flow properties of the powder depend on the morphology, PSD and density [16]. To determine the flow ability of the powder, a Ring Shear Tester RST-01.pc (Dietmar Schulze, DE) was used. This method is based on the dynamic properties of the powder and defines the flow ability under low stress conditions. This model quantifies powder flow ability with two measurable parameters, cohesion and angle of internal friction, and two derived

parameters, unconfined yield strength and major consolidation stress. The yield locus analysis is designed to determine the angle of internal friction and cohesion and then calculate the overall strength of the material under compressive load. The test consists of three parts for every point on the yield locus: consolidation, steady state and failure analysis. Plotting the failure strength of the material under different loads generates a yield locus for the sample under the pre-shear load.

2.2. Powder characterization results

Table 1 reports the chemical analysis results. The composition of the powder resulted acceptable considering the datasheet.

Table 1. Ti64 particle size distribution curves.

Element	Composition (wt%)
Al	6.40
Si	<0.05
Ti	89.77
V	3.98
Fe	0.22
O	0.14

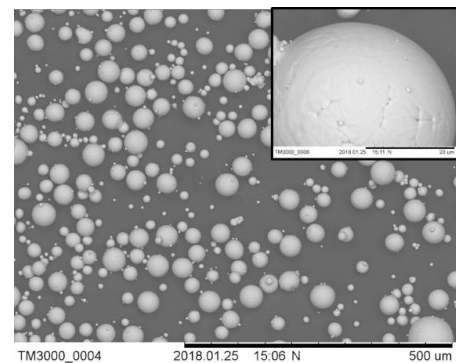The morphology of the powder particles is reported in Figure 1.

Fig. 1. SEM images of Ti64 base powder.

All powder samples showed small irregularities on some particles, but most of the particles were spherical. The PDS results are reported in Figure 2.
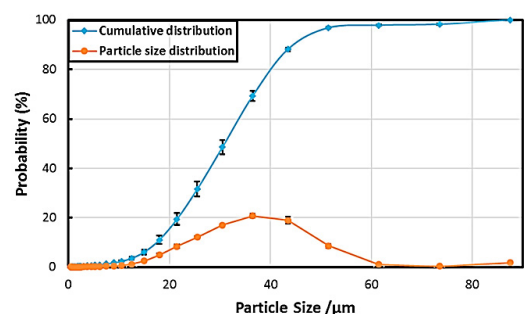

Fig. 2. Ti64 particle size distribution curves

The results are presented by integrating various spherical size coordinates with respect to their volume.

The interpolation of the graphs of the different powder samples confirms the homogeneity of the batch of powder. Since no pores or cracks in the powder particles were observed, there is no reason to believe that the powder has significant internal pores. The diagram related to the flow properties of the powder is reported in Figure 3.
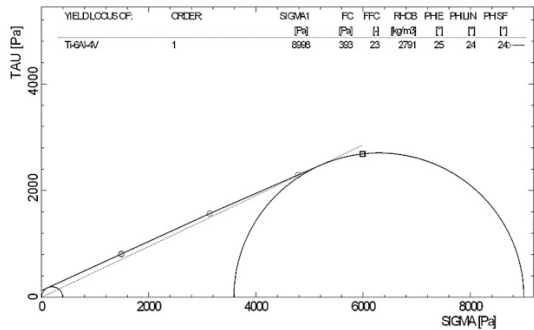

Fig. 3. Yield locus/loci curve of Ti64 powder

The results of the analysis are reported in Table 2.

Table 2. Physical properties of Ti64 powder.

Measurement	Test 1	Test 2	Units
Consolidation stress (σ_1)	8998	9030	Pa
Unconfined yield strength (σ_c or f_c)	393	394	Pa
ff$_c$ (σ_c to σ_1 ratio)	23	23	-
Bulk density	2791	2798	Kg/m^3
Effective angle of internal friction (δ or PHE)	25	26	°

The quantification of the flow behavior shows the optimal flowability (ff$_c\geq$10) of the analyzed samples of the Ti6Al4V powder used for the selective laser melting process.

2.3. SLM and post-processing

During this study the system parameters (laser power, scanning speed, hatch spacing) were kept constant, and any contamination of the powder or handling procedures that could affect powder properties were avoided.

Cubical samples (Fig. 4) of 10mm^3 were designed to produce implant models. The simple geometry of the samples was chosen to analyze the effect of different post-processing techniques applied to the top and the side surfaces resulting from the process. These sets of tests were considered to assess whether the top or size surface topography may affect the surface properties and, in turn, cellular adhesion properties of parts additively manufactured using selected laser melting (SLM). The implant models were fabricated from Ti-6Al-4V powder using a M2 Cusing SLM system (Concept Laser, Germany), which employs an Nd:YAG laser. This system operates an island scanning strategy in which the build is divided into a number of square "islands" (Fig. 4, top surface). The islands are scanned randomly and the scan direction is rotated 90° between

neighboring islands [17]. The parameters used to fabricate cylinders were 150 W laser power, 1750 mm/s scanning speed, 20 µm layer thickness, and hatch spacing of 75 µm. Support structures were not built as there was no necessity of stability during the build. Manufacture was conducted in a chamber flooded with argon gas to minimize oxygen pick-up to <0.1%.
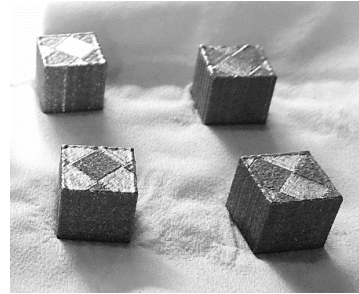

Fig. 4. Cubic SLM samples with island scanning pattern on the top surface.

As-built (AB) parts were then processed by sandblasting (SB), and vibratory finishing (VF). All the post-processing techniques were selected as the most commonly used as standard procedure in industrial SLM operations to improve the surface finish, and were applied to both the top and the side surfaces of the cubes. SB was performed in an Air Blast cabinet (CBI Equipment Ltd., UK) using a blasting gun with a compressed air regulator set to 4 bar. Silicon carbide micro grit abrasive powder with a size of 53 µm was used for sandblasting (Washington Mill Electro Minerals, UK). The sandblasting was performed for 2 min with a speed of 100 m/s on the top and side surfaces of the samples. VF was performed in a Vibratory Bowl Finishing Machine (PDJ Vibro Ltd., UK) equipped with ceramic abrasive chips (porcelain made from pure aluminum oxide ,TR-4mm) for 24 hrs at a frequency of 50Hz. Both the top surface and the side surface have been treated and analyzed.

3. Microstructure and surface structure characterization

3.1. Characterization of the samples

Secondary electron images of Ti-6Al-4V specimens were obtained using a XL30 FEG environmental SEM (Philips, UK) at 20 kV. Prior to imaging, samples were attached to an aluminum stub using adhesive carbon tabs. EDS was used to evaluate the presence of contaminants due to the post-processing.

As built and surface treated parts were analyzed using a Bruker Contour GT-K 3D Optical Microscope at 20× magnification. An area of 1 mm × 1 mm was scanned at the central point of the surface. Scanning was performed between the maximum and minimum focusing points of the z height of each sample surface. Three measurements were obtained at locations representative of the overall surface for three different sample variants.

Contact angle (CA) measurements were obtained using a Attension® Theta tensiometer (Biolin Scientific). The

samples were placed on a flat surface and deionized water (5 µm) pipetted onto the top and side surfaces. Images were captured across the horizontal plane of the droplet 60 s after application. The measurements were collected by the OneAttension software ensuring good fitting to the droplet and contact angle obtained as the inner angle between the surface and air/water interface.

3.2. SEM and Energy-dispersive X-ray spectroscopy (EDS) results

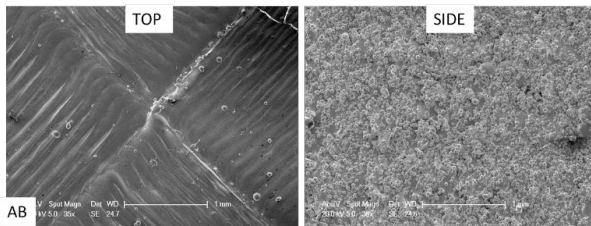The as built samples' top and side surfaces are reported in Fig. 5.

Fig. 5. SEM images of the top and side regions of Ti64 AM parts. Scale bars are 1 µm.

Scanning electron micrographs reveal the island scanning strategy used to build the parts. Spherical unmelted and partially melted particles can be observed on the side face of the AB samples.

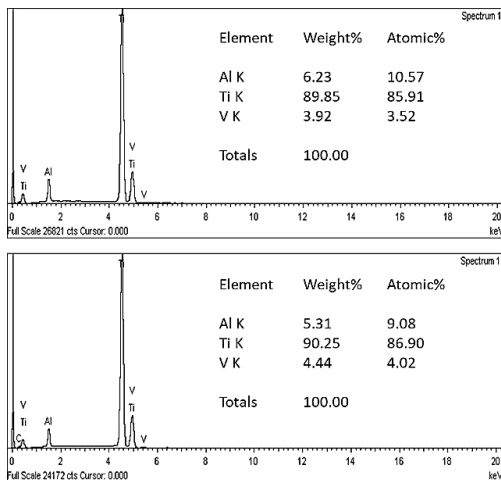Fig. 6 shows the EDS results regarding the chemical composition of the surfaces:

Fig. 6. EDS spectra of the top (up) and side (down) regions of Ti64 AM parts.

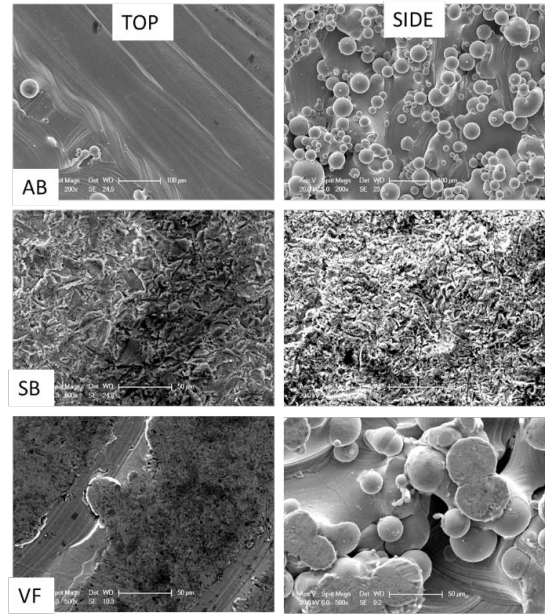Figure 7 reports the differences between the untreated as built samples and the SB and VF samples:

Fig. 7. SEM images of the top and side regions of sandblasted, vibratory finished, passivated and sandblasted with passivation Ti64 AM parts. Scale bars are 100 µm for AB samples and 50 µm for SB and VF samples.

The channels of the island patterning are still visible on the top faces of the VF samples while are not distinguishable anymore on the SB samples. No partially melted powder particles are observed after SB while a greater number of partially melted particles are still visible on the VF side face.

Table 3 show the chemical composition of the surfaces after the post processing treatments:

Table 3. Chemical composition of the samples quantified from the EDS spectra.

Sand Blasted					
Top			Side		
Element	Weight%	Atomic%	Element	Weight %	Atomic%
O K	11.26	24.7±0.9	O K	12.55	24.1±2.3
Al K	3.89	4.87	Al K	4.10	5.20
Si K	23.59	28.36	Si K	17.01	20.74
Ti K	58.12	40.96	Ti K	62.57	44.73
V K	2.71	1.79	V K	2.76	1.86
Fe K	0.43	0.26	Fe K	1.01	0.62
Vibratory finished					
Top			Side		
Element	Weight%	Atomic%	Element	Weight %	Atomic%
O K	9.67	21.07±2.4	O K	22.74	41.3±5.7
Al K	5.85	8.38	Al K	6.70	7.82
Si K	0.52	0.71	Si K	2.40	2.69
Ti K	80.32	64.79	Ti K	65.09	42.80
V K	3.64	2.76	V K	3.07	1.90

As expected, the SB treatment leads to the presence of Si on the samples especially on the side face due to the

morphology of the surface that forms several adhesion sites for the contaminants. Moreover, a small quantity of Fe is present probably due to the oxidation of the surfaces caused by the treatment as shown by the oxygen quantification results. On the other hand, a higher oxide layer resulting from the VF process is found on the side face of the samples as well as a low percentage of Si indicating a partial contamination occurring also with this treatment.

3.3. Surface roughness results

The results of the roughness analysis are presented as mean and standard deviation of the mean (Fig. 8).
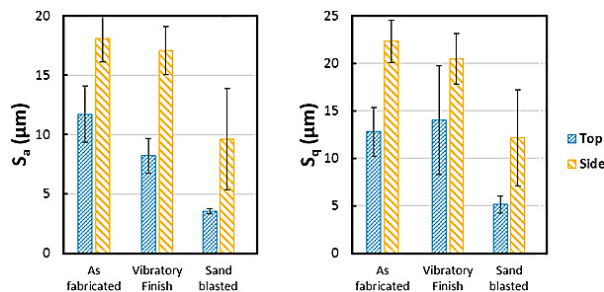

Fig. 8. Histograms of the Sa and Sq of the top and side faces of the AM samples.

No significant difference between measurements of samples as built and after vibratory finishing in relation to the Sa was highlighted. On the other hand, the SB samples demonstrated a high variability of data especially on the side face, probably due to the different effects of this process depending on the quantity of partially un-melted powder on each sample. The same effect is also observed on the Sq for both post-processing techniques. The high variance of the data is also related to both the post-processing techniques that are carried out from less controllable processes. The SB treatment significantly affected the Sa and Sq especially regarding the top face while the VF did not impact on the recorded Sa value in particular on the side face. The lower values of roughness calculated for the top and side faces of the SB samples are highly related to the morphology of the surfaces after this treatment compared to the VF ones that is characterized with higher peaks similar to the AB surfaces.

3.4. Contact angle results

The contact angle of the top and side surfaces of the as built and treated samples is reported in Figure 9 as mean and standard deviation of the mean.

These results are related to the roughness of the surfaces found in 3.2. Notably, the post processing treatments are increasing the contact angle of the surfaces enhancing the hydrophobicity of the faces. In particular, the standard deviation of the data is higher on the side surfaces related to untreated and treated samples demonstrating the variability of the process due to the presence of partially melted powder. In fact, on the top faces of the samples, the VF process is leading to lower values of CA and more hydrophilic surfaces.
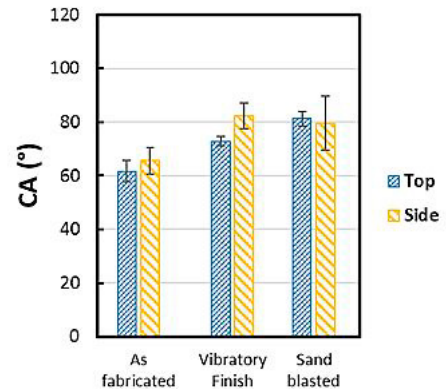

Fig. 9. Histograms of the CA of the top and side faces of the AM samples.

4. Microbiology

4.1. Bacterial adhesion tests and staining.

The ability of two different strains of bacteria to adhere on the surface of the metal samples was evaluated. Staphylococcus epidermidis (gram-positive) and Pseudomonas aeruginosa (gram-negative) to adhere to Ti64 surfaces was quantitatively assessed with crystal violet staining. This assay provided non spatially specific quantification of bacterial adhesion across the surfaces of the cubical samples (top and side faces). Ti64 samples were sterilized in 100% ethanol and allowed to dry before being placed in 24 well plates. Onto each surface, 300μm of Lysogeny broth (LB - Sigma-Aldrich, UK) for bacteria culture, inoculated 1:100 of an overnight culture of Staphylococcus aureus and Pseudomonas aeruginosa, was added. Samples were incubated at 37 °C with shaking at 25 rpm for 48 h to allow the bacterial culture. After incubation, the metallic samples were removed from the media and washed to remove any nonadherent bacteria. The samples were then prepared for the SEM and for the crystal violet staining for bacteria quantification. The culture on the samples was fixed with 4% glutaraldehyde for 10 min and washed in 20, 40, 60, 80 and 100 % ethanol (10 mins each percentage) before drying in laminar flow hood overnight. The samples were then observed under Scanning Electron Microscopy (ZEISS, USA) operating at 20kV (Fig. 10 and 11). Samples were then immersed in 1 mL of 1% (w/v) crystal violet (CV) solution for 10 min to bound the dye with the bacteria. Any unbound dye was removed by washing samples with deionized water and each sample was then transferred and immersed in 70% ethanol to solubilize the bound CV. The samples were removed and the absorbance of the remaining liquid from each sample was measured. Overnight cultures in LB were diluted to an optical density of 0.06 (600 nm). Three absorbance readings at 600 nm were obtained from each replicate using a FluoSTAR Optima plate reader (BMG Labtech).
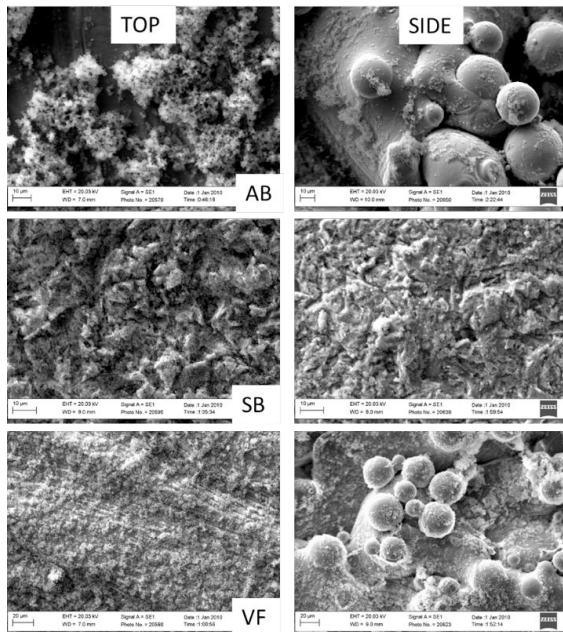
4.2. SEM images

Fig. 10. SEM images of S. epidermidis biofilms formed on the top and side regions of AB, SB and VF parts. Scale bars are 10 μm for AB and SB samples and 20 μm for VF samples.
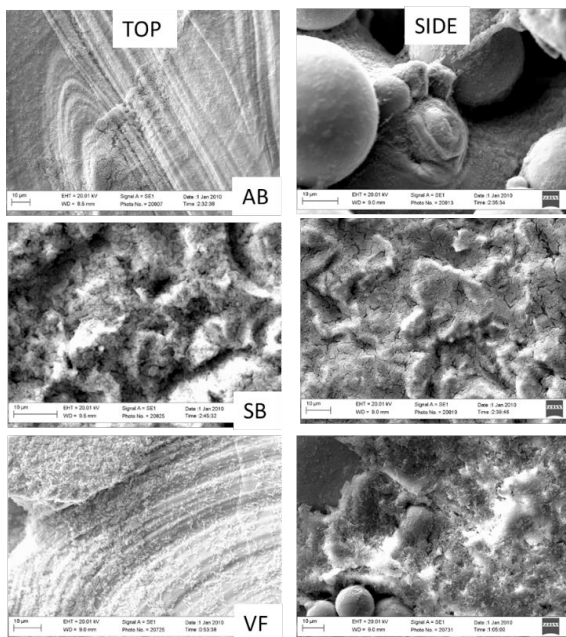

Fig. 11. SEM images of P. aeruginosa biofilms formed on the top and side regions of AB, SB and VF parts. Scale bars are 10 μm.

The SEM images show the different adhesion mechanism of the bacteria on the surfaces. In particular, the Staphylococcus epidermidis is colonizing the samples forming clumps on all the surfaces. The bacterial spatial location on the VF top surface is different from the AB ones due to the partial removal of the island pattering while the bacteria are demonstrated to adhere to the side surfaces in areas that had not been sufficiently been smoothed down. The SB samples present the same morphology on the top and side faces thus the bacterial are adhering in the same way onto the all surfaces. Regarding the Pseudomonas aeruginosa, this gram-negative bacterium colonizes the surface forming a uniform layer of biofilm. Differently from the previous case, the AB and VF top surfaces show similar results, the bacteria are seen to adhere in surface troughs of these samples, while on the side surfaces the bacteria are facilitated on the VF samples. As previously discussed, the adhesion of the bacteria is similar on the top and side surfaces of the SB samples. Moreover, in all cases, the arrangement of bacteria on the SB surfaces is notably more random compared with AB and VF. Interestingly, in the case of Pseudomonas aeruginosa, more bacteria were found onto the rough areas of the analyzed surfaces.

4.3. Crystal violet results

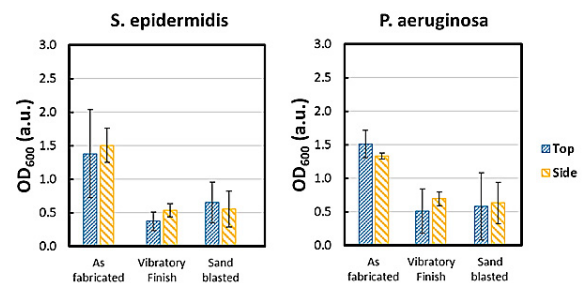The results of the CV staining are reported in Fig. 12.

Fig. 12. CV absorption of S. epidermidis and P. aeruginosa biofilms.

The results show that more bacteria, both S. epidermidis and P. aeruginosa, are adhering on the AB samples confirming the impact of the surface roughness and contact angle on the bonding sites available for the bacteria to attach. While the bacteria staining of samples allowed for adherent cells to be equally located on the top and side surface of treated samples, on the AB samples the bacteria are more located on the side face. Both strains quantifications show that the SB and VF have no significant difference on the bacteria colonization. These results combined with the high variability of the data is probably due to the poor stability of the CV staining, especially when is applied to the gram-negative bacteria.

5. Discussion

The AM manufacturing typically requires post-processing of the samples to guarantee mechanical and material properties for a certain process. Here it is demonstrated that the top and side faces of SLM samples significantly differs in terms of roughness and consequently of contact angle. The reason is related to the presence of a large amount of partially melted particles on the side face. The roughness and contact

angle of the top and side surfaces where modified by the introduction of sand blasting and vibratory finishing treatments. In particular, the AB and VF surfaces appear macroscopically similar and this may explain why no significant change was observed between the bacteria adhesion mechanism. On the other hand, the contact angle and roughness differences between AB and VF samples can clarify the different values of bacterial CV staining observed for the S. epidermidis. The SB led to an improved roughness of both the top and side surfaces of the samples by removing the partially melted particles. Accordingly, the SB surfaces shown a more hydrophobic behavior compared to the AB samples. The comparable values of CV staining demonstrated for the treated samples are mainly attributed to the less presence of partially melted spherical particles which form a large angle with the bulk surface on the SB samples. For this reason, the available surface area is maximized and the spreading of the bacterial is enhanced making the CV quantification similar to the VF samples. Moreover, contaminated blast media was embedded onto the SB surfaces, which may have increased the propensity for these surfaces to be colonized. Generally, the bacterial colonization of the surfaces is lowered by the introduction of the post-processing treatments, in particular for the S. epidermidis. The absence of a consistent trend for the CV assay of the P. aeruginosa can be due to the experimental set up of the experiments considering that CV resulted inadequate for the quantification of gram-negative bacteria.

6. Conclusions

The paper reports the possibility to alter the surface morphology and topography of additively manufactured implants by applying two of the most used post processing treatments in industry: Sand blasting and Vibratory finishing. This approach presents the opportunity to tailor implant antimicrobial properties that may be useful in dental and orthopedic implants manufacturing. It was highlighted that partially melted particles of Ti64 powder should be minimized through manufacturing optimization in order to maximize the effects of the post-processing treatments. The SB process decreased the roughness of the top and side faces of the samples reducing the differences between the top and side surfaces. The increasing prevalence of orthopedic implant infection rates highlights the need to develop parts which prevent bacterial adhesion. The bacterial organisms associated with orthopedic infections, S. epidermidis and P. aeruginosa, shown less adhesion and biofilm developments on the post-processed surfaces thus demonstrating the necessity of combine physical and chemical approaches to overcome this challenge. This preliminary study demonstrates that different postprocessing techniques may present the opportunity to tailor the properties of AM materials for specific clinical applications.

References

[1] Lowther M, Louth S, Davey A, Hussain A, Ginestra P, Carter L, Eisenstein N, Grover L, Cox S. Clinical, industrial and research prespectives on powder bed fusion additively manufactured metal implants. Additive Manufacturing 2019; 28: 565-584.

[2] Ribeiro M, Monteiro FJ, Ferraz MP. Infection of orthopedic implants with emphasis on bacterial adhesion process and techniques used in studying bacterial-material interactions. Biomatter 2012; 2(4): 176-194.

[3] Gastaldi D, Parisi G, Lucchini R, Contro R, Bignozzi S, Ginestra PS, Filardo G, Kon E, Vena P. A predictive model for the elastic properties of a collagen-hydroxyapatite porous scaffold for multi-layer osteochondral substitutes. 2015; 7(4): 1550063.

[4] Ginestra P, Ceretti E, Fiorentino A. Potential of modeling and simulations of bioengineered devices: enfoprostheses, prostheses and orthoses. Proceedings of the Institution of Mechanical Engineers Part H Journal of Engineering in Medicine 2016; 230 (7).

[5] Allegri G, Colpani A, Ginestra PS, Attanasio A. An experimental study on micro-milling of a medical grade Co-Cr-Mo alloy produced by selective laser melting. Materials 2019; 12 (13). Article number 2208.

[6] Ginestra P, Pandini S, Fiorentino A, Benzoni P, Dell'Era P, Ceretti E. Microstructured scaffold for cellular guided orientation : PCL electrospinning on laser ablated titanium collector. CIRP Journal of Manufacturing Science and Technology. 2017; 19: 147-157.

[7] Ginestra P, Fiorentino A, Ceretti E. Micro-structuring of titanium collectors by laser ablation technique: a novel approach to produce micro-patterned scaffolds for tissue engineering applications. Procedia Cirp 2017; 65: 19-24.

[8] Ferraro RM, Ginestra PS, Lanzi G, Giliani S, Ceretti E. Production of micro-patterned substrates to direct human iPSCs-derived neural stem cells orientation and interaction. Procedia Cirp 2017; 65:225-230.

[9] Ginestra PS, Madou M, Ceretti E. Production of carbonized micro-patterns by photolithography and pyrolysis. Precision Engineering 2019; 55: 137-143.

[10] Liu S, Shin YC. Additive manufacturing of Ti6Al4V alloy: A review. Materials & Design 2019; 164: 107552.

[11] Rosales-Leal JI, Rodríguez-Valverde MA, Mazzaglia G, Ramón-Torregrosa PJ, Díaz-Rodríguez L, García-Martínez O, Cabrerizo-Vílchez MA. Effect of roughness, wettability and morphology of engineered titanium surfaces on osteoblast-like cell adhesion. Colloids and Surfaces A: Physicochemical and Engineering Aspects 2010; 365(1-3): 222-229.

[12] Cox SC, Jamshidi P, Eisenstein NM, Webber MA, Burton H, Moakes RJ, Grover LM. Surface finish has a critical influence on biofilm formation and mammalian cell attachment to additively manufactured prosthetics. ACS Biomaterials Science & Engineering 2017; 3(8): 1616-1626.

[13] Brouqui P, Rousseau MC, Stein A, Drancourt M, Raoult D. Treatment of Pseudomonas aeruginosa-infected orthopedic prostheses with ceftazidime-ciprofloxacin antibiotic combination. Antimicrobial agents and chemotherapy 1995; 39(11), 2423-2425.

[14] Chouirfa H, Bouloussa H, Migonney V, Falentin-Daudré C. Review of titanium surface modification techniques and coatings for antibacterial applications. Acta biomaterialia 2019; 83:37-54.

[15] Janson O, Gururaj S, Pujari-Palmer S, Ott MK, Strømme M, Engqvist H, Welch K. Titanium surface modification to enhance antibacterial and bioactive properties while retaining biocompatibility. Materials Science and Engineering: C 2019; 96: 272-279.

[16] Thejane K, Chikosha S, du Preez WB. Characterisation and monitoring of Ti6AL4V (ELI) powder used in different selective laser melting systems. South African Journal of Industrial Engineering 2017; 28 (3): 161-171.

[17] Qiu C, Adkins NJ, Attallah MM. Microstructure and tensile properties of selectively laser-melted and of HIPed laser-melted Ti−6Al−4V. Mater. Sci. Eng. 2013; 578: 230-239.